Wave Packet Simulation of Nonadiabatic Dynamics in Highly Excited 1,3-Dibromopropane

Rasmus Y. Brogaard,[†] Klaus B. Møller,*[,‡] and Theis I. Sølling[†]

Center for Molecular Movies, Department of Chemistry, University of Copenhagen, Universitetsparken 5, DK-2100 København Ø, Denmark, and Center for Molecular Movies, Department of Chemistry, Technical University of Denmark, DTU 207, DK-2800 Lyngby, Denmark

Received: June 16, 2008; Revised Manuscript Received: August 04, 2008

We have conducted wave packet simulations of excited-state dynamics of 1,3-dibromopropane (DBP) with the aim of reproducing the experimental results of the gas-phase pump−probe experiment by Kötting et al. [Kötting, C.; Diau, E. W.-G.; Sølling, T. I.; Zewail, A. H. *J. Phys. Chem. A* **2002**, *106*, 7530]. In the experiment, DBP is excited to a Rydberg state 8 eV above the ground state. The interpretation of the results is that a torsional motion of the bromomethylene groups with a vibrational period of 680 fs is activated upon excitation. The Rydberg state decays to a valence state, causing a dissociation of one of the carbon bromine bonds on a time scale of 2.5 ps. Building the theoretical framework for the wave packet propagation around this model of the reaction dynamics, the simulations reproduce, to a good extent, the time scales observed in the experiment. Furthermore, the simulations provide insight into how the torsion motion influences the bond breakage, and we can conclude that the mechanism that delays the dissociation is solely the electronic transition from the Rydberg state to the valence state and does not involve, for example, intramolecular vibrational energy redistribution (IVR).

1. Introduction

The real-time investigation of molecular motion in a chemical reaction is the ultimate goal of the femtochemistry discipline. This goal is achieved by using a fs pulse to generate a superposition of vibrational eigenstates, a wave packet that exhibits a time-dependent behavior.[1] It is this property that makes it possible to probe nuclear motion. In some cases, the initially activated dynamics includes unreactive nuclear motions that influence the reactive degrees of freedom.[2−8] An example of such a behavior is found in the fs pump−probe experiment on gaseous 1,3-dibromopropane (DBP) done by Kötting et al.[9]The decay of the number of parent molecules can be fitted to a single exponential with a decay time of 2.5 ps. The fragment resulting from a carbon−bromine bond breakage exhibits a corresponding rise time. The most fascinating aspect of the experiment is that an oscillation is superimposed on the experimental signal. The authors ascribe this to the creation of a wave packet by a two-photon excitation onto an $n \rightarrow 5p$ Rydberg state 8 eV above the ground state. The wave packet consists of vibrational eigenstates of a low-frequency symmetrical torsion motion of the two bromomethylene groups. The vibration, which corresponds well to a ground-state normal mode,[9] is sketched in Figure 1. The motion of the wave packet along the torsion coordinate can be followed by ionization with the probe pulse.[9] Thus, the interpretation of the experiment is that the period of the oscillations of 680 fs corresponds to the vibrational period of the torsion motion. Ab initio calculations show[9] that the Rydberg state is crossed by an $n \rightarrow \sigma^*$ valence state which is repulsive in the carbon−bromine bond stretching coordinate. Thus, the bond breakage is believed to occur after a transition from the bound Rydberg state to the repulsive valence state. This model of the reaction dynamics is sketched in Figure 2.

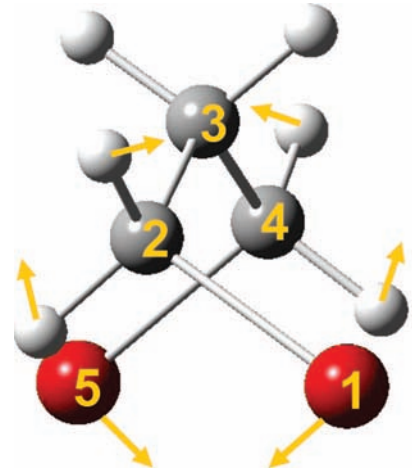

Figure 1. The symmetrical torsion motion.

The aim of this work is to (semi)quantitatively reproduce the measured time scales by conducting wave packet simulations in the framework of the above-presented model to support the interpretation of Kötting et al.[9]

Although creating the link between theory and experiment in DBP is an interesting problem in itself, the reaction dynamics of DBP also represents a case of general interest. DBP is a representative of molecular systems that are characterized by the fascinating property of being potentially reactive systems exhibiting unreactive motion interleaving the reactive dynamics. The bottleneck that guides from the unreactive to the reactive dynamics can be electronic transitions[2−4,7,8] or intramolecular vibrational energy redistribution (IVR).[5,6] In the case of DBP, it is not possible from the experimental data to judge whether the process that delays the bond breakage also involves IVR. Such detailed insights into the dynamics can be provided by a wave packet simulation.

* To whom correspondence should be addressed. E-mail: klaus.moller@kemi.dtu.dk.
[†] University of Copenhagen.
[‡] Technical University of Denmark.

10.1021/jp805273w CCC: $40.75
Published on Web 09/27/2008

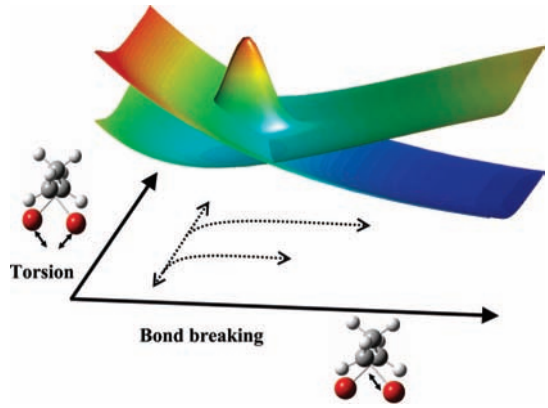

Figure 2. Sketch describing the reaction dynamics as interpreted from the results of the DBP experiment.

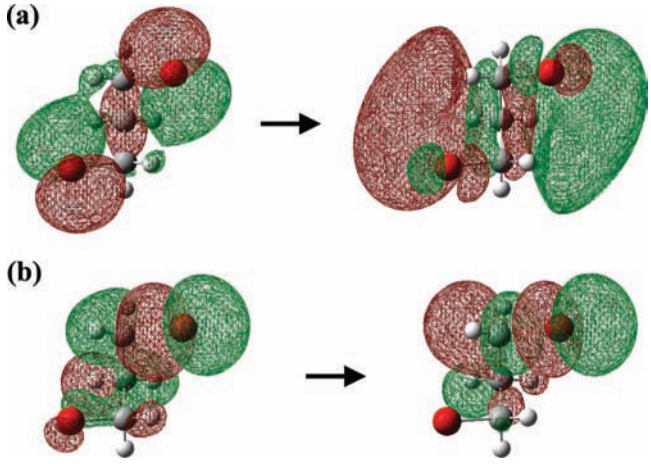

Figure 3. The Kohn−Sham orbitals involved in the excitations $n_1 \rightarrow 5p_x$ (a) and $n_2 \rightarrow \sigma^*$ (b) leading to the Rydberg and valence state, respectively.

Simulating the complex behavior of DBP presents a challenge and demands the use of state-of-the-art methods. In this respect, we have been inspired by the recent work on nonadiabatic wave packet dynamics of the photodissociation of bromoacetyl chloride done by Lasorne et al.[10] and develop the theoretical framework for DBP in a similar way. The theoretical setup is presented in section 2. Computational details regarding the implementation of the model are presented in section 3. The wave packet simulations are presented and discussed in section 4, and section 5 ends the paper with concluding remarks and outlook.

2. Theoretical Setup

The model of the DBP reaction dynamics described in the preceding section presents a significant reduction in the dimensionality of the problem; only 2 out of a total of 27 vibrational degrees of freedom and 2 out of many electronic states[9] are considered. The simplicity of the model is a beauty but also makes one wonder if it is possible to reproduce the experimental results in such a simple framework; the reaction dynamics might involve parameters essential for a theoretical description that were not probed in the experiment. The aim of the present work is not to achieve a quantitative correspondence between simulation and experiment using a complex model. Instead, we want to investigate how adequately the simple model can describe the experimental results. This section describes how we set up the theoretical framework for the wave packet propagations.

The corner stone in wave packet simulations is the time-dependent Schrödinger equation

$$i\hbar\frac{\partial}{\partial t}\mathbf{\Psi}(\mathbf{q},t) = \mathbf{H}\mathbf{\Psi}(\mathbf{q},t) \tag{1}$$

where the Hamiltonian **H** consists of a kinetic and a potential energy operator. We start out by defining the nuclear coordinates **q** and the corresponding kinetic energy operator (KEO). In section 2.3, we define the representation of the electronic states and the potential energy operator (PEO). For simulating the C−Br dissociation, we include in the Hamiltonian a complex absorbing potential (CAP), which will be described in section 2.4. In section 2.5, we end the description of the theoretical setup by defining the equations of motion that are solved in the wave packet propagation.

2.1. Nuclear Coordinates. In simulating molecular dynamics, treating all internal nuclear coordinates of the system in a fully quantum mechanical way quickly becomes computationally prohibitive as the size of the system increases. The coordinates can be divided into a set of active coordinates **q** each of which is associated with an ab initio calculated potential energy surface (PES) $V(\mathbf{q}, \mathbf{Q}(\mathbf{q}))$ and a set $\mathbf{Q}(\mathbf{q})$ of inactive coordinates considered as functions of the active ones.[11] The active coordinates in this work are the C−Br bond stretching coordinate (R) and the torsion coordinate (D). We have only considered the asymmetric stretch of a single C−Br bond as a symmetric stretch would lead to products of extremely high energy (trimethylene and two bromine atoms). Moreover, in such systems where the symmetric dissociation of two bonds is possible, the initial activation of a symmetric stretching will eventually lead to branching into two asymmetric dissociations;[12] here, we consider only one of them as they will lead to identical products. The value of the D coordinate is defined as the dihedral angle $\delta(\mathrm{Br}^1\mathrm{C}^2\mathrm{C}^3\mathrm{C}^4)$ (see Figure 1), which is kept equal to $\delta(\mathrm{C}^2\mathrm{C}^3\mathrm{C}^4\mathrm{Br}^5)$ to ensure the symmetry of the torsion. The internal coordinates of the H atoms bonded to C^2 and C^4 will be defined such that D describes the torsion of the bromomethylene groups.

As the D coordinate corresponds to the lowest frequency normal mode of DBP, it is reasonable to adopt the approximation that all inactive coordinates relax instantaneously during the torsion motion. We therefore model DBP as an adiabatically constrained system in which the inactive coordinates are adjusted to the actives ones.[11]

2.2. The Kinetic Energy Operator. The KEO can be expressed in the active coordinates as follows[13]

$$\hat{T}_n(\mathbf{q}) = \sum_{ij} f_2^{ij}(\mathbf{q})\frac{\partial^2}{\partial q_i\,\partial q_j} + \sum_i f_1^i(\mathbf{q})\frac{\partial}{\partial q_i} + v(\mathbf{q}) \tag{2}$$

where $v(\mathbf{q})$ is an extrapotential term that arises from the choice of normalization convention of the wave function. In this work, we will use the TNUM program[14,15] that implements the algorithm of Lauvergnat and Nauts for evaluating the f_2, f_1, and v functions numerically exact.[13] The power of TNUM is that it allows for the definition of **q** in terms of curvilinear coordinates. Furthermore, the inactive coordinates **Q** are implicitly taken into account in the calculation of the KEO. The inactive coordinates can be treated in several ways, among which are the rigid (frozen) and adiabatically constrained models.[13] These properties of TNUM are especially valuable for this work as the alternative, an analytical definition of the KEO, would be rather complex for a system at the size of DBP.

2.3. Electronic States. The representation of the electronic states is very important in describing nonadiabatic molecular dynamics because of the coupling between the states. In the

TABLE 1: The optimized parameters of the functions used to fit the raw diabatic PESs (values in a.u.)

state	parameters								
1	A	α	R^{eq}	D_2^{eq}	E_1	a_1	b_1	c_1	d_1
	0.1050	0.8628	3.751	0.7990	0.2881	0.07260	−0.06320	−0.1077	0.1286
2	B	β		D_2^{eq}	E_2	a_2	b_2	c_2	d_2
	5.752	1.137	1.362	0.2227	0.01108	0.1007	0.2538	0.1394	

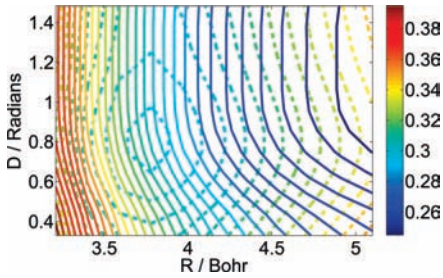

Figure 4. Isoenergy contours (in hartree) of the diabatic PESs of the Rydberg state (dotted lines) and the valence state (full lines).

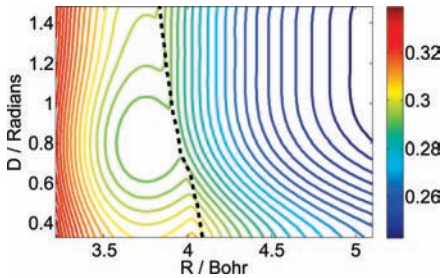

Figure 5. Energy contours (in hartree) of the lower adiabatic PES. The diabatic seam obtained from the scans of the adiabatic PESs along the R coordinate (see text) is shown as a dotted black line.

TABLE 2: Parameters Used in the Wave Packet Propagation (values in au)

parameter	R	D
init. center	3.761	1.135
init. width	0.2	0.1
CAP starting point	4.79	
Grid min	3.213	0.3316
Grid max	5.102	1.588
no. of basis functions	55	80
no. of grid points	70	100

adiabatic representation, the derivative operators in the KEO are responsible for the coupling.[16] In regions of the PES with strongly avoided crossings, this derivative coupling can change very abruptly by a small change in geometry, and in the case of a conical intersection, the coupling even diverges.[17] Therefore, it is often more convenient to use a representation in which the derivative coupling vanishes, a diabatic representation. For polyatomic molecules, this is not possible to achieve, but an approximate or quasidiabatic representation in which the derivative coupling is negligible can be constructed.[18] In the diabatic representation, the coupling between the electronic states is represented as a potential coupling in the PEO.[16]

In this work, two approximately diabatic states are constructed in a way that follows the ideas of Ruedenberg and Atchity.[19] We form diabatic states from adiabatic ones, requiring uniformity of the electronic character throughout the nuclear coordinate space, thereby ensuring a vanishing derivative coupling. Thus, naming the electronic states as Rydberg and valence in the Introduction was implicitly an adoption of a diabatic representation; the names refer to the uniform electronic configuration of the diabatic states. In the following, we number the Rydberg state as state 1 and the valence state as state 2.

2.4. Complex Absorbing Potential. The implementation of an optical or complex absorbing potential (CAP) in the Hamiltonian is a useful strategy for simulating dissociative degrees of freedom.[20,21] In this work, we use a CAP for absorbing the wave function in the asymptotic region of the R coordinate, thereby simulating the C−Br bond breakage. The CAP has the following simple form

$$\hat{W}(R) = \begin{cases} -i(R - R_d)^2 & R \geq R_d \\ 0 & R < R_d \end{cases} \quad (3)$$

where R_d is the starting point of the CAP.

2.5. Equations of Motion. In the wave packet propagations done in this work, we solve the time-dependent Schrödinger equation, eq 1, in the diabatic representation of the electronic states. Thus, $\mathbf{\Psi}(\mathbf{q}, t)$ is a vector representing the nuclear wave packets in the Rydberg and valence state, and $\mathbf{H}$ is the matrix of Hamiltonian operators in the diabatic electronic representation. The diagonal elements of this matrix define the Hamiltonian for the isolated diabatic state $i = 1, 2$ as $H_{ii} = \hat{T}_n(\mathbf{q}) + V_{ii}(\mathbf{q}, \mathbf{Q}(\mathbf{q})) + \hat{W}(R)$, and the off-diagonal elements $H_{ij} = V_{ij}(\mathbf{q}, \mathbf{Q}(\mathbf{q}))$ define the coupling between the states. The functions V_{ij} $(i, j = 1, 2)$ are the matrix elements of the PEO in the diabatic electronic representation.

3. Computational Details

All ab initio calculations are done using the Gaussian 98 program package.[22] According to electron diffraction studies, DBP is most stable in the gauche−gauche conformation.[23] As in the work of Kötting et al., the gauche−gauche conformation will therefore be the starting point of the calculations.

3.1. Nuclear Coordinates and the Kinetic Energy Operator. We have implemented the adiabatically constrained model by optimizing the ground-state geometry of DBP as a function of R and D using B3LYP/6-31+G(d). Although the rigorous approach would be to relax the coordinates in the excited state, we believe that relaxing them at the ground state is better than freezing the coordinates. By inspecting every inactive coordinate, we find that only some are varying significantly. Thus, we consider as adiabatically constrained the coordinates $\angle(Br^1C^2C^3)$, $\angle(C^2C^3C^4)$, and $\angle(C^3C^4Br^5)$. These coordinates are among the ones that exhibit the largest standard deviation (2.6-4.7%) relative to their mean value for $1.7 \leq R \leq 2.4$ Å and $19° \leq D \leq 85°$. The three valence angles increase as the D coordinate decreases to compensate for the repulsion between the bromine atoms. The rest of the inactive coordinates are considered frozen at the ground-state equilibrium geometry for the gauche−gauche conformation.

When implementing adiabatically constrained coordinates in TNUM, the exact derivatives up to third order with respect to the active coordinates have to be known.[13] Thus, the values of the adiabatically constrained coordinates have to be fit to an

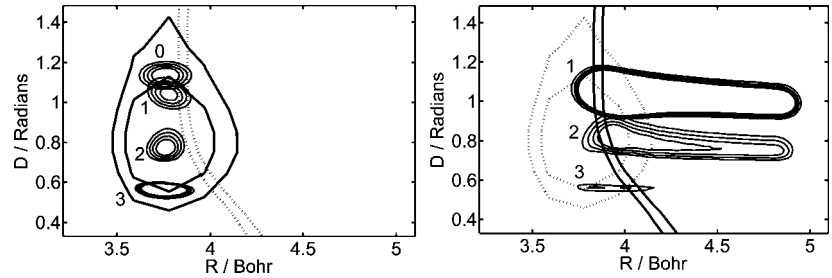

Figure 6. Isodensity contours of the wave packets $|\Psi_1(R, D, t)|^2$ (left) and $|\Psi_2(R, D, t)|^2$ (right). The contour levels are {12, 16, 20, 24} au for Ψ_1 and {0.018, 0.024, 0.030, 0.036} au for Ψ_2. Also shown are isoenergy contours at {0.293, 0.297} hartree for the diabatic PES. The snapshots are separated by 4000 au (97 fs).

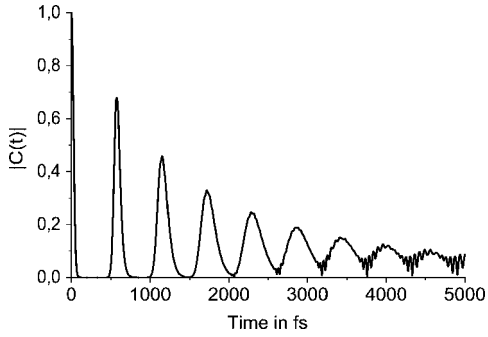

Figure 7. The absolute value of the autocorrelation function, eq 7.

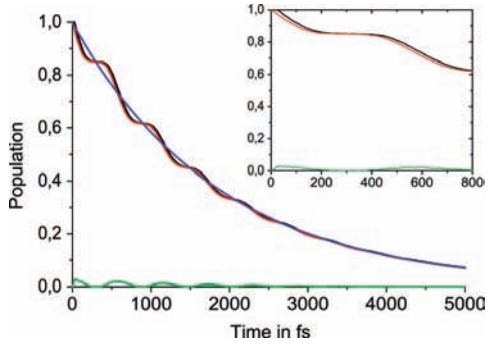

Figure 8. The Rydberg (red), valence (green), and total (black) population as a function of time. The blue curve is the best fit of the total population to a single exponential decay.

analytical expression. Here, we have used independent third-order polynomials in R and D.

By inspecting the behavior of the f_2^{ij} functions, it can be possible to simplify the expression in eq 2 by approximating the f_2^{ij} functions by constants if their variation is low.[10] To preserve the hermiticity of the KEO, this means that the f_1^i functions have to be set to zero. The complexity of the KEO is then significantly reduced because it no longer depends on $\mathbf{q}$. In the present case, this approximation is not valid as the f_2^{ij} functions for the coordinates R and D are far from being constant. We have therefore used the varying functions in the wave packet simulations.

3.2. The Diabatic PESs. This section describes the way the PESs corresponding to the approximately diabatic Rydberg and valence states are constructed. Assuming two-photon excitation and comparing the experimental photon energy with the calculation of the excited states of DBP using TDB3LYP/6-31+G(d), Kötting et al. claim that the orbitals involved in the transition to the initially excited state are the lone pair n_1 and the Rydberg $5p_x$ orbitals shown in Figure 3a.[9] From the calculation of excited-state PESs along the R coordinate, Kötting et al. find that the Rydberg state is crossed by an $n_2 \rightarrow \sigma^*$ valence state; the orbitals involved are shown in Figure 3b. Because of the symmetry of DBP, the n_2 and σ^* orbitals are pairwise quasidegenerate when the C−Br bond lengths are equal. However, for geometries in which the bond lengths differ, the orbitals can (to a certain extent) be assigned to each of the bonds. Thus, the orbitals shown in Figure 3b are associated with a geometry where the C−Br bond around which the orbitals are localized is the longest one. This is in good agreement with intuition in that the lone-pair electron that is involved in the bond breakage is excited from the bromine that is repelled from the rest of the molecule.

Kötting et al. calculated the excited states in 1D scans along the R and D coordinate.[9] To get the diabatic PESs needed in this work, we calculate the excited states of DBP along the full two-dimensional (R,D) grid used in the wave packet propagation. We have performed these ab initio calculations following Kötting et al. in using TDB3LYP/6-31+G(d) to calculate the excited states of ground-state geometries optimized using B3LYP/6-31+G(d).

From the calculated excited states, we want to select the ones having the most $n_1 \rightarrow 5p_x$ character to get the diabatic PES of the Rydberg state. Whereas the Rydberg $5p_x$ orbital is virtually unaltered by changes in the geometry, the opposite is true for the bromine lone-pair orbitals that interact extensively with each other. We therefore first selected the states that arise from excitation from each of the four highest-lying lone-pair orbitals (DBP has a total of six lone pairs, three on each bromine atom) into the Rydberg $5p_x$ orbital. By inspecting the Kohn−Sham orbitals involved, we chose the excitation energies that correspond to the states having the most $n_1 \rightarrow 5p_x$ character. The sum of these energies and the corresponding ground-state energies constitute a raw form of the diabatic PES of the Rydberg state. The selection of excitation energies is not always unambiguous, though. For nearly symmetrical geometries where the stretched C−Br bond is no longer than about 2.2 Å, the identification of the n_1 orbital among the four lone-pair orbitals is possible. However, for longer bond lengths, the identification becomes ambiguous. In such cases, we chose the state with the excitation energy that resulted in the smoothest form of the raw PES.

A raw form of the diabatic PES of the $n_2 \rightarrow \sigma^*$ valence state was constructed in a similar way. Here, we first selected states arising from excitation from the two lowest-lying lone pairs to the two C−Br antibonding orbitals of DBP. From these states, we selected the ones with the most $n_2 \rightarrow \sigma^*$ character. In ambiguous cases, the excitation energies that resulted in the smoothest PES were chosen.

The raw diabatic PESs were fitted to the following analytical expressions

$$V_{11}(R, D) = A(1 - e^{-\alpha(R-R^{eq})})^2 + P_1(D - D_1^{eq})$$
$$V_{22}(R, D) = Be^{-\beta R} + P_2(D - D_2^{eq}) \quad (4)$$

which represent the R coordinate by a Morse oscillator in the Rydberg state and an exponentially repulsive potential in the valence state. The D coordinate is represented by an anharmonic potential $P_i(q) = E_i + a_iq^2 + b_iq^3 + c_iq^4 + d_iq^5$ in both states. The optimized parameters are found in Table 1. Figure 4 shows the energy contours of the diabatic PESs.

3.3. The Diabatic Coupling. As noted above, the interaction between two electronic states is represented as a potential coupling $V_{12}(\mathbf{q}, \mathbf{Q}(\mathbf{q}))$ in the diabatic representation. We approximate the diabatic coupling by a constant V_{12}. This section describes how the value of the constant is determined.

In including only the Rydberg and the valence state in the model, we have neglected the coupling to all other electronic states and treated DBP as a two-state system. In such a system, the relation between the adiabatic and diabatic PESs is[24]

$$\Delta V^{adia} = \sqrt{(\Delta V^{dia})^2 + 4(V_{12})^2} \quad (5)$$

where ΔV^{adia} and ΔV^{dia} refer to the energy gap between the adiabatic and diabatic PESs, respectively. For geometries in which the diabatic PESs cross, that is, $\Delta V^{dia} = 0$, eq 5 reduces to $\Delta V^{adia} = 2V_{12}$. At these geometries, the value of the diabatic potential coupling V_{12} is thus proportional to the energy gap between the adiabatic PESs. This simple way of estimating V_{12} is exploited by scanning the R coordinate in very small steps as to locate the point where the energy gap between the adiabatic PESs is smallest. To select the right adiabatic states among the many states present, we inspect the electronic character of the states just as when constructing the approximately diabatic PESs. The two-state approximation is, of course, a very rough one, and the interaction between the adiabatic PESs corresponding to the Rydberg and valence diabatic states is influenced by nonadiabatic interaction with other states. We try to level out this effect by doing the scan for several values of the D coordinate representing the entire range of the grid used in the wave packet simulations and approximate V_{12} by the average of the coupling values obtained from the different scans. This gives a value of V_{12} of 4.0×10^{-4} hartree. The lower adiabatic PES obtained from the diabatic PESs with this value of V_{12} is depicted in Figure 5. Also shown in the figure is the diabatic crossing seam as obtained from the scans. We see that, although the construction of the diabatic PESs and coupling is quite approximate, the crossing seam of the fitted PESs is in good agreement with the one obtained from the ab initio data.

4. Wave packet Propagations

The wave packet propagations were done using the ElVibRot program,[25,26] which is interfaced with TNUM. The wave function was discretized on a grid using the discrete variable representation (DVR) of the wave function.[27] We used a Fourier basis set for the R coordinate and sine functions as the basis set for the D coordinate. These basis functions resulted in an equidistant DVR grid in both coordinates. In solving eq 1, the Chebychev polynomial expansion of the evolution operator was used.[28] The propagations were done using a time step of 1.2 fs and a total propagation time of 5 ps.

According to the model of the DBP dynamics, the initially excited state is the Rydberg state, and therefore, the initial diabatic wave packet vector $\Psi^0(R, D)$ only has a component in state 1. Using the Condon approximation and the ultrashort duration of the pump pulse, the initial wave packet on the Rydberg state is well approximated by the vibrational ground-state wave function of the electronic ground state.[24] Approximating the vibrations of DBP by harmonic oscillators, the initial wave packet is proportional to a product of Gaussian functions in the R and D coordinates[29]

$$\Psi_1^0(R, D) \propto e^{-(R - R_0/\sigma_R)^2} e^{-(D - D_0/\sigma_D)^2} \quad (6)$$

The centers R_0 and D_0 of the Gaussian functions are chosen according to a ground-state geometry optimization of DBP using B3LYP/6-31G(d). The width parameters σ_R and σ_D are chosen somewhat arbitrarily but are similar to the results obtained from a relaxation propagation[30] that we have conducted on the ground-state PES calculated using B3LYP/6-31+G(d). Table 2 collects the parameters used in the propagation.

4.1. Results and Discussion. Figure 6 shows isodensity contours of the two diabatic nuclear wave packets $|\Psi_1(R, D, t)|^2$ and $|\Psi_2(R, D, t)|^2$ in time intervals of 4000 au (97 fs) after the start of the propagation. The left part of Figure 6 shows the wave packet in the Rydberg state moving along the torsion coordinate for approximately half of the vibrational period. The right part of Figure 6 shows the corresponding evolution of the wave packet in the valence state which will be discussed later. In the second half of the period, the behavior of the wave packets is virtually reversed and therefore not shown. The simulated vibrational period of the torsion coordinate D is derived from the autocorrelation function

$$C(t) = \langle \Psi^0 | \Psi(t) \rangle \quad (7)$$

Figure 7 shows the absolute value of the function. A closer look reveals that it peaks at multiples of 578 fs, which is thus the simulated vibrational period of the torsion motion. This is in quite good agreement with the experimentally observed 680 fs with a deviation of 15%. We observe that the width of the peaks of the autocorrelation increases for each recurrence. This dephasing of the wave packet is caused by the anharmonicity of the potential in the D coordinate. The broadening of the wave packet influences the decay dynamics of the Rydberg state, which we will discuss in the following.

The simulated time scale for the bond breakage can be derived from the populations shown in Figure 8. When part of the wave packet is transferred from the Rydberg to the valence state, it gets absorbed by the CAP very fast (~40 fs) compared to the time scale of the transfer. Therefore, the population of the valence state is kept at a minimum, and the total population (norm) is thus virtually equivalent to the Rydberg population $\langle \Psi_1(t) | \Psi_1(t) \rangle$. Fitting the total population to a single exponential decay gives a decay time of 1.9 ps. Considering the simple model of the diabatic PESs and coupling, this is in good agreement with the experimentally observed time of 2.5 ps with a deviation of 24%.

The results presented so far show that the wave packet simulation reproduces the experimental time scales to a good extent. To obtain further insight into the dissociation process, we conducted a propagation including only the lower adiabatic PES. In this case, the dissociation occurs within less than 50 fs, corresponding to motion on an effectively repulsive surface. This shows that it is the nonadiabatic trapping of the wave packet in the bound Rydberg diabatic state that delays the dissociation.

We can further elaborate on the mechanism of the dissociation by noticing the step-like feature superimposed on the single exponential decay of the Rydberg population shown in Figure 8. The feature is caused by the topology of the diabatic PESs as shown in Figure 6; in the Franck−Condon region of the PES,

the wave packet is close to the diabatic crossing seam. However, because the diabatic crossing seam is not exactly parallel to the *D* coordinate, the distance to the crossing seam increases as the wave packet moves along the *D* coordinate away from the Franck−Condon region. It therefore experiences that the effect of the diabatic coupling is decreasing. Thus, the rate of population transfer from the Rydberg to the valence state and thereby the rate of dissociation decreases. When completing a vibrational period and returning to the starting position, the wave packet experiences an increasing effect of the diabatic coupling, and the rate increases. We can therefore conclude that the rate of bond breakage depends on the motion along the torsion coordinate only as far as regards the electronic coupling and thus that IVR is *not* involved in the photodissociation of DBP.

For longer time scales than that shown in Figure 6, the broadening of the wave packet mentioned above means that it experiences an averaged effect of the diabatic coupling of a larger region of the PES along the *D* coordinate. The decay rate is therefore correspondingly averaged. This levels out the step-like feature in the decay of the Rydberg state, which, after about 3 ps, is virtually a plain single exponential decay; see Figure 8.

4.2. Remarks Regarding the KEO. We have tried to increase the number of adiabatically constrained inactive coordinates from the three valence angles mentioned in section 3.1, but it does not influence the propagation; the results are virtually the same. This shows that the construction of the KEO is "converged" in the sense that the rest of the inactive coordinates can effectively be considered as frozen.

It is also interesting to note that we get similar results to the ones reported above (vibrational period: 718 fs; decay time: 2.3 ps) by considering all inactive coordinates frozen in the construction of the KEO, although such a KEO is inconsistent with the construction of the PESs from relaxed coordinates.

Even when approximating the f^{ij}_2 functions, which are far from being constant, by their average value on the (*R*,*D*) grid and setting the f^{i}_1 functions (and v) to zero, we obtain results close to the ones reported above (vibrational period: 546 fs; decay time: 2.1 ps).[31]

5. Conclusion and Outlook

By conducting wave packet simulations within the framework of the interpretation model of Kötting et al.,[9] we have been able to reproduce the results of the DBP experiment to a good extent; with a simulated period of the torsional vibration of 578 fs and a time scale for C−Br bond breakage of 1.9 ps, the deviation from the experimental results is within 24%. Of course, this does not prove that the model is correct, but the simulation results support the validity of the model. Besides, the wave packet simulations have added further insight into the dynamics as they show that the dissociation is limited by the coupling of two PESs; the motion along the torsion coordinate influences the effect of the coupling and thus the dissocation.

Hence, the dissociation of DBP is similar to the one observed in pump−probe experiments on NaI in which the wave packet oscillates in a bound PES and dissociates in the region of the PES where the coupling to a repulsive PES is significant.[2−4] The dynamics of DBP is a little more complex in that the oscillation of the wave packet which influences the coupling to the repulsive PES takes place along a nonreactive coordinate perpendicular to the dissociation coordinate.

Acknowledgment. The authors thank Dr. David Lauvergnat for kindly providing the programs TNUM and ElVibRot. R.Y.B. wishes to express his deepest gratitude to Dr. Lauvergnat for invaluable help and advice in using the programs. Financial support from the Carlsberg Foundation and the Danish National Research Foundation is acknowledged.

References and Notes

(1) Zewail, A. H. *Angew. Chem., Int. Ed.* **2000**, *39*, 2586.
(2) Rose, T. S.; Rosker, M. J.; Zewail, A. H. *J. Chem. Phys.* **1988**, *88*, 6672.
(3) Mokhtari, A.; Cong, P.; Herek, J. L.; Zewail, A. H. *Nature* **1990**, *348*, 225.
(4) Møller, K. B.; Henriksen, N. E.; Zewail, A. H. *J. Chem. Phys.* **2000**, *113*, 10477.
(5) Hennig, S.; Engel, V.; Schinke, R.; Nonella, M.; Huber, J. R. *J. Chem. Phys.* **1987**, *87*, 3522.
(6) Nonella, M.; Huber, J. R.; Untch, A.; Schinke, R. *J. Chem. Phys.* **1989**, *91*, 194.
(7) Guo, H.; Zewail, A. H. *Can. J. Chem.* **1994**, *72*, 947.
(8) Sølling, T. I.; Diau, E. W.-G.; Kötting, C.; De Feyter, S.; Zewail, A. H. *ChemPhysChem* **2002**, *3*, 79.
(9) Kötting, C.; Diau, E. W.-G.; Sølling, T. I.; Zewail, A. H. *J. Phys. Chem. A* **2002**, *106*, 7530.
(10) Lasorne, B.; Bacchus-Montabonel, M.-C.; Vaeck, N.; Desouter-Lecomte, M. *J. Chem. Phys.* **2004**, *120*, 1271.
(11) Gatti, F.; Justum, Y.; Menou, M.; Nauts, A.; Chapuisat, X. *J. Mol. Spectrosc.* **1997**, *181*, 403.
(12) Møller, K. B.; Zewail, A. H. *Chem. Phys. Lett.* **1998**, *295*, 1.
(13) Lauvergnat, D.; Nauts, A. *J. Chem. Phys.* **2002**, *116* (19), 8560.
(14) Lauvergnat, D. *TNUM, fortran90 program*, 2001.
(15) Lauvergnat, D.; Baloïtcha, E.; Dive, G.; Desouter-Lecomte, M. *Chem. Phys.* **2006**, *326*, 500.
(16) May, V.; Kühn, O. *Charge and Energy Transfer Dynamics in Molecular Systems*; Wiley-VCH: New York, 2000.
(17) Domcke, W., Yarkony, D. R., Köppel, H., Eds. *Conical Intersections: Electronic Structure, Dynamics and Spectroscopy*; World Scientific Publishing Co. Pte. Ltd.: River Edge, NJ, 2004.
(18) Mead, C. A.; Truhlar, D. G. *J. Chem. Phys.* **1982**, *77*, 6090.
(19) Ruedenberg, K.; Atchity, G. J. *J. Chem. Phys.* **1993**, *99*, 3799.
(20) Leforestier, C.; Wyatt, R. E. *J. Chem. Phys.* **1983**, *78*, 2334.
(21) Kosloff, R.; Kosloff, D. *J. Comput. Phys.* **1986**, *63*, 363.
(22) Frisch, M. J.; Trucks, G. W.; Schlegel, H. B.; Scuseria, G. E.; Robb, M. A.; Cheeseman, J. R.; Zakrzewski, V. G.; Montgomery Jr., J. A.; Stratmann, R. E.,; Burant, J. C.; Dapprich, S.; Millam, J. M.; Daniels, A. D.; Kudin, K. N.; Strain, M. C.; Farkas, O.; Tomasi, J.; Barone, V.; Cossi, M.; Cammi, R.; Mennucci, B.; Pomelli, C.; Adamo, C.; Clifford, S.; Ochterski, J.; Petersson, G. A.; Ayala, P. Y.; Cui, Q.; Morokuma, K.; Rega, N.; Salvador, P.; Denneberg, J. J.; Malick, D. K.; Rabuck, A. D.; Raghavachari, K.; Foresman, J. B.; Cioslowski, J.; Ortiz, J. V.; Baboul, A. G.; Stefanov, B. B.; Liu, G.; Liashenko, A.; Piskorz, P.; Komaromi, I.; Gomperts, R.; Martin, R. L.; Fox, D. J.; Keith, T.; Al-Laham, M. A.; Peng, C. Y.; Nanayakkara, A.; Challacombe, M.; Gill, P. M. W.; Johnson, B.; Chen, W.; Wong, M. W.; Andres, J. L.; Gonzalez, C.; Head-Gordon, M.; Replogle, E. S.; Pople, J. A. *Gaussian 98*, revision A.11.3; Gaussian, Inc.: Pittsburgh, PA, 2002.
(23) Farup, P. E.; Stølevik, R. *Acta Chem. Scand. A* **1974**, *28a*, 680.
(24) Tannor, D. J. *Introduction to Quantum Mechanics—A Time-Dependent Perspective*; University Science Books: New York, 2007.
(25) Lauvergnat, D. *ElVibRot*, quantum dynamics code; 2006; http://www.lcp.u-psud.fr/Pageperso/lauvergnat/perso/.
(26) Ndong, M.; Lauvergnat, D.; Chapuisat, X.; Desouter-Lecomte, M. *J. Chem. Phys.* **2007**, *126*, 244505.
(27) Light, J. C.; Hamilton, I. P.; Lill, J. V. *J. Chem. Phys.* **1985**, *82*, 1400.
(28) Tal-Ezer, H.; Kosloff, R. *J. Chem. Phys.* **1984**, *81*, 3967.
(29) Atkins, P.; Friedman, R. *Molecular Quantum Mechanics*, 4th ed.; Oxford University Press Inc.: New York, 2005.
(30) Kosloff, R.; Tal-Ezer, H. *Chem. Phys. Lett.* **1986**, *127*, 223.
(31) This propagation was performed using the MCTDH program.[32−34]
(32) (a) Worth, G. A.; Beck, M. H.; Jäckle, A.; Meyer, H.-D. *The MCTDH Package*, version 8.2; University of Heidelberg: Heidelberg, Germany, 2000. (b) Meyer, H.-D. *The MCTDH Package*, version 8.3; 2002; See http://www.pci.uni-heidelberg.de/tc/usr/mctdh/.
(33) Beck, M. H.; Jäckle, A.; Worth, G. A.; Meyer, H.-D. *Phys. Rep.* **2000**, *324*, 1.
(34) Meyer, H.-D.; Manthe, U.; Cederbaum, L. S. *Chem. Phys. Lett.* **1990**, *165*, 73.

JP805273W